Fermi National Accelerator Laboratory

FERMILAB-Conf-96/379

DØ

High-E_T Jet Results from DØ

Nikos Varelas
For the DØ Collaboration
Michigan State University
East Lansing, Michigan 48824

Fermi National Accelerator Laboratory
P.O. Box 500, Batavia, Illinois 60510

November 1996

Submitted to the *28th International Conference on High Energy Physics (ICHEP '96)*, Warsaw, Poland, July 25-31, 1996.

Disclaimer

Distribution

HIGH-E_T JET RESULTS FROM DØ

Nikos Varelas
(for the DØ Collaboration)

Michigan State University, East Lansing, Michigan 48824, USA

Recent results on jet physics from the DØ experiment at the Fermilab Tevatron Collider are reported. Recent data taken from 1994 - 1995 in $p\bar{p}$ collisions at $\sqrt{s} = 1.8$ TeV have been analysed; preliminary measurements of the central inclusive jet cross section, the dijet mass spectrum, and the dijet angular distribution are presented and compared with next-to-leading order QCD predictions.

1 Introduction

High transverse momentum jets are predominantly produced in $p\bar{p}$ collisions by two body scattering of a single proton constituent with an antiproton constituent. Next-to-leading order (NLO) QCD predictions which include the possibility of a third radiated parton have been available for quite some time.[1,2,3] These calculations to third order in the strong coupling constant (α_s^3) reduce theoretical uncertainties to 10-20% . We measure the cross section for the production of jets as a function of the jet transverse energy, the dijet mass spectrum, and the dijet angular distribution in the DØ detector[4] at the Fermilab Tevatron Collider at $\sqrt{s} = 1.8$ TeV. These measurements, when compared to NLO QCD predictions, constitute a rigorous test of QCD. Previous measurements of the inclusive jet production,[5] dijet mass distribution,[6] and the dijet angular distribution[7] have been presented by the CDF collaboration.

2 Jet Detection

Jet detection in DØ relies primarily on the excellent linearity and fine transverse and longitudinal segmentation of the uranium–liquid argon calorimeters, which cover pseudorapidity $|\eta| \leq 4.1$ ($\eta = -\ln\tan(\theta/2)$, where θ is the polar angle relative to the proton beam). The calorimeters have electromagnetic and hadronic single particle resolutions of $15\%/\sqrt{E(\mathrm{GeV})}$ and $50\%/\sqrt{E(\mathrm{GeV})}$, respectively. They are transversely segmented into projective towers of $\Delta\eta \times \Delta\phi = 0.1 \times 0.1$ and have longitudinal segmentation of eight to eleven segments depending on η. The electromagnetic modules include the first four longitudinal segments and the coarse hadronic modules the final longitudinal segment. The intervening segments comprise the fine hadronic modules and the intercryostat detectors. The total calorimetric depth exceeds seven nuclear interaction lengths for $|\eta| \leq 0.5$. The calorimeters are also segmented into trigger tiles of $\Delta\eta \times \Delta\phi = 0.8 \times 1.6$ and trigger towers of $\Delta\eta \times \Delta\phi = 0.2 \times 0.2$, where ϕ is azimuthal angle. The event vertex is determined using tracks reconstructed in the central tracking system. The detector includes two trigger scintillator hodoscopes located on each side of the interaction region at $1.9 < |\eta| < 4.3$. Timing distributions of particles traversing the two hodoscopes indicate the occurrence of a single inelastic interaction or of multiple inelastic interactions during a single beam–beam crossing.

On-line event selection occurred in two hardware stages and a final software stage. The initial hardware trigger selected an inelastic particle collision as indicated by the hodoscopes. The next trigger stage required transverse energy above a preset threshold in the calorimeter trigger tiles for 1994–1995 data and towers for the 1992–1993 data. Selected events were digitized and sent to an array of processors. Jet candidates were then reconstructed with a fast cone algorithm and the entire event logged to tape if any jet E_T exceeded a specified threshold. During the 1994–1995 (1992–1993) data run, the software jet thresholds were 30, 50, 85, and 115 (20, 30, 50, 85, 115) GeV with integrated luminosities of 0.355, 4.56, 51.7 and 90.7 (0.00950, 0.0778, 1.02, 7.95, and 13.7) pb^{-1}, respectively.

3 Reconstruction and Off-line Selection

Jets were reconstructed off-line using an iterative jet cone algorithm with a cone radius of $\mathcal{R}$=0.7

in η–ϕ space.[8] Background jets from isolated noisy calorimeter cells and accelerator losses were eliminated with quality cuts. Background events from cosmic ray bremsstrahlung were eliminated by requiring the missing E_T in an event to be less than 70% of the leading jet E_T. Residual contamination from the backgrounds is estimated to be less than 2% at all $E_T < 500$ GeV based on Monte-Carlo simulations and scanning of all very high jet E_T candidates.[9] The overall jet selection efficiency for $|\eta| \leq 0.5$ has been measured as a function of jet E_T and found to be 97±1% below 250 GeV and 94±1% at 400 GeV.

At high instantaneous luminosity more than one interaction in a single beam crossing is probable. The event reconstruction retained, at most, two vertices. The quantity $\mathcal{H}_T = |\Sigma_{\rm jets}\vec{E}_T^{\rm jet}|$ was calculated for both vertices. The vertex with the minimum $\mathcal{H}_T$ was selected as the event vertex and used to calculate jet E_T and η. This reduced the cross section 5% at 100 GeV and 10% at 300 GeV. The $\mathcal{H}_T$ was also taken as $\not\!\!E_T$ for the cosmic ray cut described earlier, when choosing the secondary vertex. This procedure was not required for the 1992–1993 data set as the instantaneous luminosity was much lower. The selected vertex was required to be within 50 cm of the detector center. The z requirement was 90 ± 1% efficient, independent of E_T.

The transverse energy of each jet was corrected for offsets due to underlying events and noise/zero suppression, out-of-cone showering, and detector hadronic response as determined from the missing transverse energy balance of photon-jets events.[10] Figure 1 shows the mean total jet correction as a function of E_T for $|\eta| \leq 0.5$.

4 Inclusive Jet Cross Section

The inclusive jet cross section corrected for jet and event selection efficiency is shown in Fig. 2. The observed E_T spectrum has been corrected for resolution smearing by assuming a trial unsmeared spectrum, $(AE_T{}^{-B}) \cdot (1 - 2E_T/\sqrt{s})^C$, and fitting its convolution with the measured resolution to the measured cross section. The data are plotted with their (uncorrelated) statistical errors; in addition, there is an overall luminosity uncertainty of 8%. The inset shows the total systematic uncertainty (without the luminosity uncertainty) as

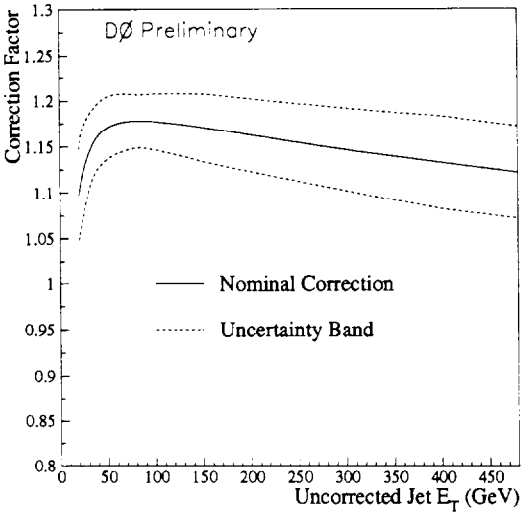

Figure 1: The jet energy scale correction factor as a function of uncorrected E_T. The upper and lower curves represent the total uncertainty.

a function of E_T which is dominated by the energy scale uncertainty.

Figure 2 also shows a prediction of the inclusive jet cross section from the NLO parton event generator JETRAD.[1] The NLO calculation requires specification of the renormalization and factorization scale ($\mu = E_T/2$ where E_T is the maximum jet E_T in the generated event), parton distribution function (pdf) (CTEQ2ML,[11]) and the parton clustering algorithm. Partons within $1.2\times\mathcal{R}$ of one another were clustered if they were also within $\mathcal{R}$=0.7 of their E_T weighted η, ϕ centroid. The value of $1.2\times\mathcal{R}$ was determined by overlaying jets from separate events and determining the separation at which the jet reconstruction algorithm could resolve the individual jets.

The theoretical predictions have uncertainties associated with the above choices of pdf, μ scale, and parton clustering algorithm. Variation of the pdf can alter the prediction by 10-20% depending on E_T. Variation of μ between $0.25\,E_T$ and $2\,E_T$ can alter the theoretical normalization by $\sim$ 10%. In addition, if we had evaluated the μ scale by selecting the E_T of each jet (instead of selecting the E_T of the leading jet) the calculated cross section would have increased by $\sim$ 5% at low E_T values. Finally the choice of parton clustering between $1.2\times\mathcal{R}$ and $2.0\times\mathcal{R}$ alters the normalization

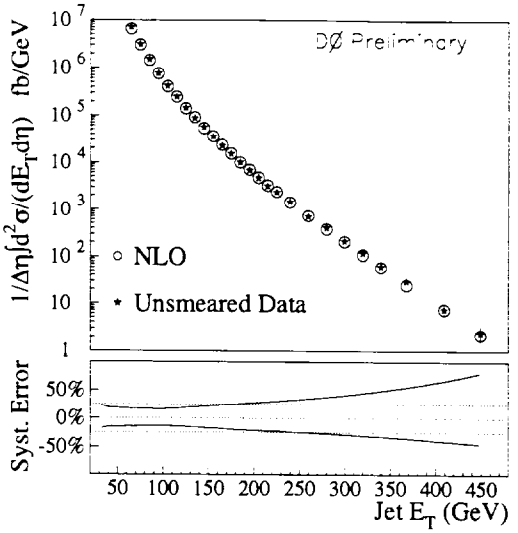

Figure 2: A comparison of the central inclusive cross section for the 1994–95 data sample (91 pb^{-1}) to a NLO calculation. The points include statistical errors. The inset curves represent plus and minus 1σ systematic error.

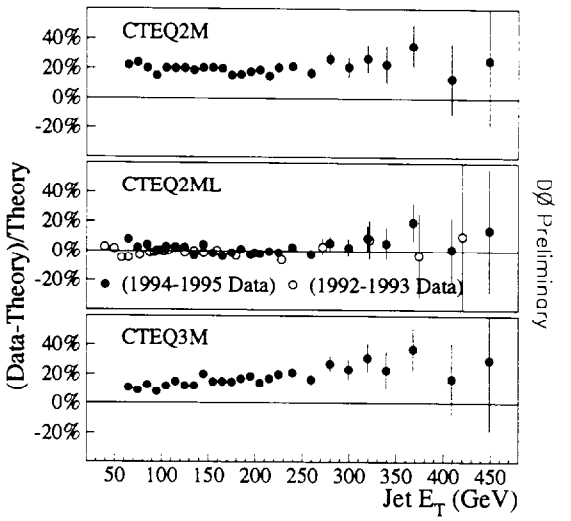

Figure 3: Difference between the data and three QCD predictions normalized to the theoretical prediction $((D-T)/T)$. The solid (open) symbols are for the 1994–1995 (1992–1993) data.

above 50 GeV by $\sim$ 5% with a small (2–3%) E_T dependence.

Figure 3 shows the ratio, $(D-T)/T$, for the data (D) and NLO theoretical (T) predictions based on the CTEQ2M, CTEQ2ML, and CTEQ3M pdf's.[11] The shapes of both the CTEQ2M and CTEQ2ML predictions are in excellent agreement with the data, as is the CTEQ2ML normalization. The 1992–1993 data, also shown in the central figure, are in excellent agreement with the 1994–1995 data and the CTEQ2ML prediction.

5 Inclusive Dijet Mass Distribution

The inclusive dijet mass cross sections are computed for two partially overlapping pseudorapidity ranges: $|\eta|_{1,2} < 1.0$, with $\Delta\eta < 1.6$, and $|\eta|_{1,2} < 0.5$, for the contiguous sets of mass ranges 200 – 270 – 370 – 500 and 200 – 220 – 330 – 420 GeV, corresponding to the various software jet thresholds. The final observed cross section corrected for jet and event selection efficiency is shown in Fig. 4. The combined systematic errors are also shown, ranging from $\sim$13% at 200 GeV to $\sim$55% at 950 GeV. The systematic error is dominated by the uncertainty due to the energy scale.

Figure 4 also shows a comparison to the predictions of JETRAD. The NLO calculation of the dijet mass spectrum has been smeared by the measured jet resolutions. There is good agreement between the prediction and the data over seven orders of magnitude. Figure 5 shows the ratio, $(D-T)/T$, for the data (D) and the NLO predictions based on the CTEQ2ML[11] and MRSD0'[12] pdf's. Given the experimental and theoretical uncertainties the predictions are in excellent agreement with the data. The CTEQ2ML pdf gives the best agreement for the absolute normalization.

6 Dijet Angular Distribution

The dijet angular distribution allows us to measure the properties of parton-parton scattering without strong dependence on the details of the parton distribution functions; since all three classes of scattering processes are dominated by t-channel gluon exchange, the angular dependences of the $qg \to qg$, $q\bar{q} \to q\bar{q}$, and $gg \to gg$ processes are similar.

The dijet angular distribution is typically expressed in term of χ, where $\chi = (1+\cos\theta^*)/(1-\cos\theta^*) = e^{|\eta_1-\eta_2|}$. This is done in order to flatten out the t-channel pole contribution to the distribution and to facilitate an easier comparison to

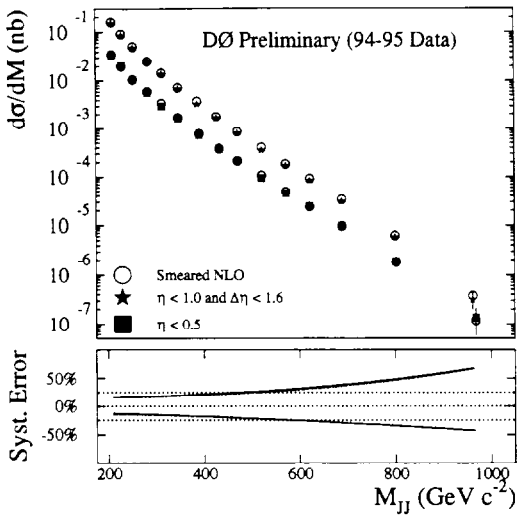

Figure 4: $d\sigma/dM_{jj}$ for $|\eta|_{1,2} < 1.0$, $\Delta\eta < 1.6$ ($|\eta|_{1,2} < 0.5$). The inset solid (dash-dot) curves represent the $\pm 1\sigma$ systematic errors (the dotted lines show the 0, $\pm 25\%$ levels).

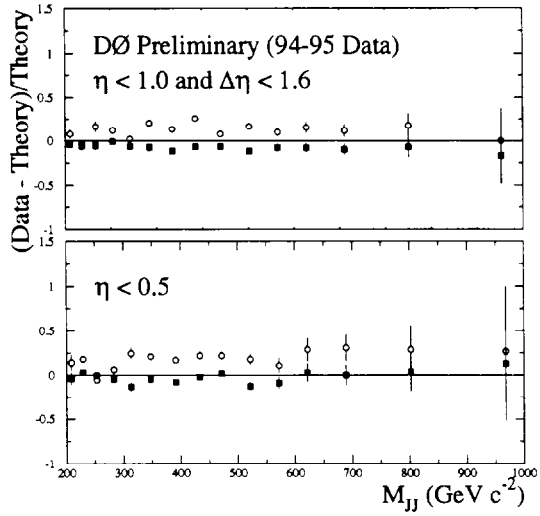

Figure 5: The difference between the data and the smeared NLO QCD predictions normalized to the theoretical prediction ($(D-T)/T$). The solid (open) symbols represent the calculation using the CTEQ2ML (MRSD0′) pdf's.

the predictions of QCD. It also allows signatures of new physics that might have a more isotropic angular distribution than QCD (e.g., quark compositeness) to be more easily examined as they would produce an excess at low values of χ.

The quantity measured in the dijet angular analysis is $1/N(dN/d\chi)$, for given ranges of the dijet mass. The two leading E_T jets were required to have a maximum pseudorapidity less than 3.0. For the mass bins and χ values presented, a cut on $|\eta_{\rm boost}| = \frac{1}{2}|(\eta_1 + \eta_2)| < 1.5$ was applied to ensure uniform acceptance.

The dijet angular distribution is relatively insensitive to many systematic effects; in particular it shows little dependence on variation of the overall energy scale. However, since χ depends on $\Delta\eta$ directly, it is sensitive to η dependent quantities. The effects of multiple interactions and a possible η dependent energy scale are the two dominant sources of error in this analysis, contributing $\sim 8\%$ and $\sim 10\%$ respectively.

The leading order and next to leading order theory predictions were calculated using JETRAD. The CTEQ3M parton distribution functions were used with a renormalization scale of $E_T/2$ of the leading E_T jet. The theory was smeared in E_T and η in order to compare it to data; the effect of E_T and η smearing is small. Four mass ranges are shown compared to the LO and NLO predictions of QCD in Fig. 6. We see that the NLO predictions are in a good agreement with the data. Finally, Fig. 7 demonstrates the effects of varying the renormalization/factorization scale at NLO on the dijet angular distributions. For the scale values studied, only a small deviation from the NLO predictions is observed.

7 Conclusion

In conclusion, we have measured the inclusive jet cross section, the dijet mass spectrum, and the dijet angular distribution. As can be seen the QCD predictions are in excellent agreement with our measurements. The QCD NLO model, using different pdf's, describes the E_T- dependent shape of the observed central inclusive jet cross section over seven orders of magnitude and within experimental and theoretical uncertainties agrees well in absolute normalization. The inclusive dijet mass spectrum is in very good agreement with the QCD NLO model, and the same holds true for the dijet angular distribution which agrees very well with QCD NLO predictions in all mass bins. These DØ measurements should provide a strong constraint

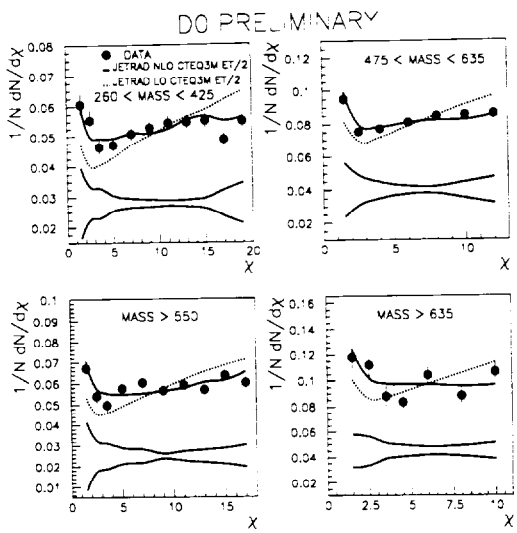

Figure 6: Comparisons of data to NLO and LO predictions of QCD using JETRAD with CTEQ3M and a renormalization scale of $E_T/2$. The errors bars are statistical. Shown at the bottom of each plot is the $\pm 1\sigma$ systematic error band.

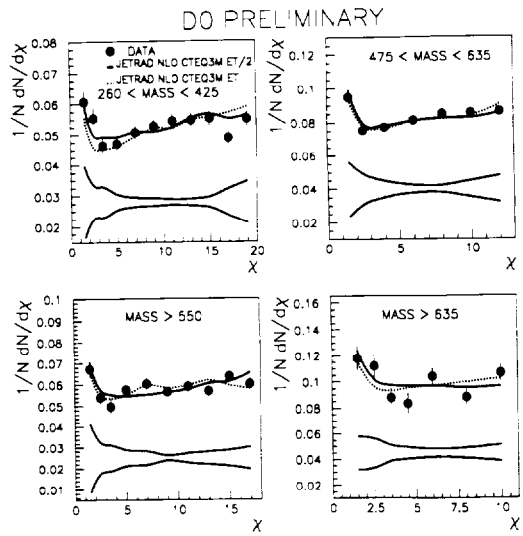

Figure 7: Comparisons of data to NLO predictions of QCD using JETRAD with CTEQ3M and renormalization scales of $E_T/2$ and E_T.

on the uncertainties of the current theoretical predictions.

Acknowledgments

We thank W.Giele, E.Glover, and D.Kosower for their helpful comments and suggestions. We thank the staffs at Fermilab and the collaborating institutions for their contributions to the success of this work, and acknowledge support from the funding agencies in the U.S., France, Russia, Brazil, India, Colombia, Mexico, Korea and Argentina.

References

1. W. T. Giele, E. W. N. Glover, and D. A. Kosower, *Phys. Rev. Lett.* **73**, 2019 (1994) and private communications.
2. S. D. Ellis, Z. Kunszt, and D. E. Soper, *Phys. Rev. Lett.* **64**, 2121 (1990).
3. F. Aversa *et al.*, *Phys. Rev. Lett.* **65**, 401 (1990).
4. S. Abachi *et al.*, (DØ Collaboration), *Nucl. Instrum. Methods* **A338**, 185 (1994).
5. F. Abe *et al.*, (CDF Collaboration), *Phys. Rev. Lett.* **70**, 1376 (1993); *Phys. Rev. Lett.* **77**, 438 (1996).
6. F. Abe et al., (CDF Collaboration), *Phys. Rev.* **D41**, 1722 (1990).
7. F. Abe et al., (CDF Collaboration), *Phys. Rev. Lett.* **69**, 2896 (1992); A. Bhatti, *Inclusive Jet Production at Tevatron, Fermilab-Conf-95-192-E*, Jun 1995. 12pp. Presented at 10th Topical Workshop on Proton-Antiproton Collider Physics, Batavia, IL, 9-13 May 1995.
8. S.Abachi *et al.*, (DØ Collaboration), *Phys. Lett.* **B357**, 500 (1995).
9. D.Elvira, Ph.D. Thesis, Universidad de Buenos Aires, Buenos Aires, Argentina (1995).
10. R. Kehoe, in the Proceedings of the VIth International Conference on Calorimetry in High Energy Physics, Laboratori Nazionali di Frascati, Frascati, Italy, June 8-14, 1996.
11. J.Botts *et al.*, (CTEQ Collaboration), *Phys. Rev.* **D51**, 4763 (1995); *Phys. Lett.* **B304**, 159 (1993).
12. A.D.Martin, R.G.Roberts, and W.J.Stirling, *Phys. Lett.* **B306**, 145 (1993); and erratum *Phys. Lett.* **B309**, 492 (1993).